$Ni_3Cr_2P_2Q_9$ (Q = S, Se): New Quaternary Transition Metal Chalcogenides with a Unique Layered Structure

Michael A. McGuire[†,‡] and Francis J. DiSalvo*[,§]

Department of Physics, Clark Hall, and Department of Chemistry and Chemical Biology, Baker Laboratory, Cornell University, Ithaca, New York 14853

Received March 27, 2007. Revised Manuscript Received April 30, 2007

The new transition metal chalcogenides $Ni_3Cr_2P_2S_9$ and $Ni_3Cr_2P_2Se_9$ have been discovered and characterized. Single-crystal X-ray diffraction studies of the selenide reveal a new layered structure type (space group $P6_3/m$, $a = 6.244(4)$ Å, $c = 18.479(19)$ Å, $Z = 2$, $R_1 = 0.0235$). Powder X-ray diffraction and electron microprobe analysis suggest that the sulfide is isostructural to the selenide and that a solid solution forms between them. The layers are composed of transition metal centered octahedra with chalcogenides at the vertices which are joined in pairs by face sharing along the *c*-direction. These units share edges to form honeycomb layers in the *ab*-plane with linear P−Ni−P units in the holes of the honeycomb nets. Transport properties measurements from 80−300 K on single crystals with compositions $Ni_3Cr_2P_2S_{9-x}Se_x$ ($x = 0$, 3, 6) revealed activated behavior in electrical resistivity ($E_a = 0.02-0.03$ eV, $\rho_{300K} = 50-220$ mΩ·cm) and positive values of the Seebeck coefficient ($S_{300K} = 80-225$ μV/K), showing that these compounds behave like p-type semiconductors. Magnetization measurements on $Ni_3Cr_2P_2S_9$ single crystals from 5 to 400 K reveal antiferromagnetic interactions between the transition metal ions and an ordering transition near 105 K.

Introduction

We have been investigating multinary chalcogenides as thermoelectric materials, because they tend to form small band gap semiconductors often with complex crystal structures. These two characteristics can be important in determining the utility of a thermoelectric material, which is determined by its figure of merit $Z = S^2/\rho\kappa$. Here S is the Seebeck coefficient or thermopower, ρ is the electrical resistivity, and κ is the thermal conductivity.

Most good thermoelectric materials are doped semiconductors, and it can be shown that the best thermoelectric performance is expected for band gaps that are close to $10k_BT$, where k_B is Boltzmann's constant and T is the average temperature of operation.[1] This means that band gaps near 0.25 eV are optimal for cooling devices operated near room temperature. In the expression for Z derived for semiconducting materials, all of the microscopic materials properties other than the band gap and dopant concentration appear in the combination referred to as the B factor.[1−3] For transport along the x direction, B is dependent upon the mobility μ_x, the effective masses m_i, the number of degenerate conduction or valence band extrema N_c, and the lattice thermal conductivity κ_L in the following way: $B \sim N_c\mu_x(m_xm_ym_z)^{1/2}/\kappa_L$. Materials with complex crystal structures containing many atoms per unit cell can have lower lattice thermal conductivities, since the thermal energy is shared among the three heat carrying acoustic phonon modes and the numerous optical phonon modes ($3N - 3$ where N is the number of atoms per primitive unit cell) which do not carry heat effectively.[4] Complex crystal structures can also lead to increased values of N_c by producing multiple nearly degenerate band extrema (within k_BT of each other) and by exactly degenerate extrema that are automatically generated by symmetry when the extrema lie away from the center of the Brillouin zone (the maximal degeneracy occurs when an extremum occurs at a general point in the Brillouin zone and is equal to the number of point symmetry operations of the crystal class). The latter can significantly increase N_c in high-symmetry crystal structures.[1]

Much of our synthetic work targeting improved thermoelectric materials has been of an exploratory nature, because we believe that large improvements in thermoelectric performance are most likely to come through the discovery of new materials, rather than modifications of known compounds. In particular, we have explored the idea of biasing new crystal structures toward high symmetry by using starting materials with high symmetry building blocks, like SiS_4 or PS_4 tetrahedral units. Reactions between $CrPS_4$ and elemental Ni and S led to the discovery of a new quaternary phase $Ni_3Cr_2P_2S_9$. Further studies revealed that a selenide analogue also exists. Single crystal and powder X-ray diffraction studies show that these compounds adopt a new layered structure type with the composition $Ni_3Cr_2P_2Q_9$ (Q = S, Se). These compounds do adopt a high-symmetry crystal structure, but do not retain the tetrahedral building blocks present in the starting material $CrPS_4$, and can in fact be made by direct reaction of the elements. In addition to

* To whom correspondence should be addressed. E-mail: fjd3@cornell.edu.
† Department of Physics.
‡ Current address: Department of Chemistry, Frick Laboratory, Princeton University, Princeton, NJ 08544, USA.
§ Department of Chemistry.

(1) Mahan, G. *J. Appl. Phys.* **1989**, *65*, 1578.
(2) Sofo, J.; Mahan, G. *Phys. Rev. B* **1994**, *49*, 4565.
(3) Hicks, L.; Dresselhaus, M. *Phys. Rev. B.* **1993**, *47*, 12727.
(4) Slack, G. A. *Solid State Phys.* **1979**, *34*, 1.

10.1021/cm070849f CCC: $37.00
Published on Web 08/10/2007

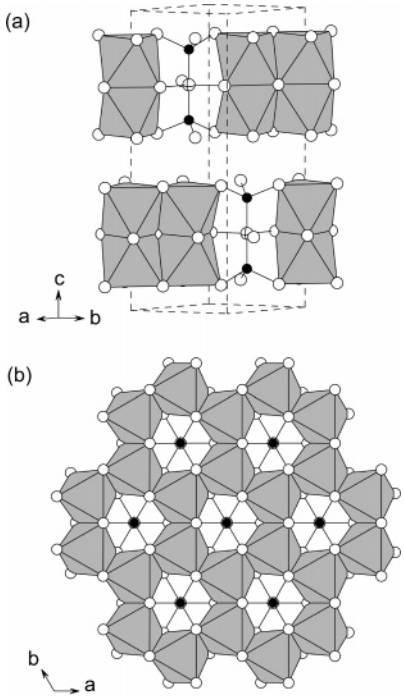

Figure 1. Crystal structure of $Ni_3Cr_2P_2Se_9$. Se is white, P is black, M(3) is crossed, and M(1) and M(2) are at the centers of the gray octahedra (see text for details regarding occupancy of M sites). The dotted lines outline the hexagonal unit cell. The layered nature of the structure is emphasized in part a, while part b shows a single layer viewed along the *c*-axis.

the structural analysis, we present and discuss here results from transport property (electrical resistivity and Seebeck coefficient) and magnetic susceptibility measurements. Brief descriptions of the experimental procedures are noted in the presentation and discussion of the results below. Further details of the syntheses and the characterization techniques employed can be found in the Supporting Information.

Results and Discussion

Crystal Structure of $Ni_3Cr_2P_2Se_9$. Reaction of the elements in stoichiometric or near stoichiometric ratios at 700−800 °C followed by slow cooling produce crystals of the title compounds as black plates in the shape of hexagons and half-hexagons. Figure 1 shows the crystal structure of $Ni_3Cr_2P_2Se_9$ determined by single-crystal X-ray diffraction analysis. The results of the structure refinement are listed in Table 1.[5] Atomic positions and anisotropic displacement parameters are given in the Supporting Information. The structure contains layers of edge sharing octahedra which form a honeycomb network, with transition metal (M) sites at the centers of the octahedra and Se at the vertices, similar to the layers seen in $NiPS_3$.[6] Two such layers are fused together by face sharing of the octahedra. In the holes of the honeycomb net are linear P−M−P units, with each of the three atoms bonded to three Se atoms. Thus the P atoms are in fourfold coordination, and this M atom is in a trigonal bipyramidal environment. The coordination environments and interatomic distances are shown in Figure 2.

(5) The cif file for Ni3Cr2P2Se9 may also be obtained from Fachinformationszentrum Karlsruhe, 76344 Eggenstein-Leopoldshafen, Germany (fax (+49)7247-808-666; e-mail crysdata@fiz-karlsruhe.de) on quoting the deposition number CSD-417894.

(6) Ouvrard, G.; Brec, R.; Rouxel, J. *Mater. Res. Bull.* **1985**, *20*, 1181.

Table 1. Single-Crystal Refinement Results for $Ni_3Cr_2P_2Se_9$

empirical formula	$Ni_3Cr_2P_2Se_9$
temperature	175(5) K
wavelength	0.71073 Å
crystal system, space group	hexagonal, $P6_3/m$
unit cell dimensions	a = 6.244(4) Å
volume	623.9(8) Å^3
Z, calculated density	2, 5.603 g/cm^3
crystal size	0.080 × 0.060 × 0.008 mm^3
θ range	2.20−33.12°
limiting indices	$-7 \le h \le 9$
	$-8 \le k \le 6$
	$-27 \le l \le 28$
reflection collected/unique	7546/824 [R_{int} = 0.0636]
completeness to θ_{max}	99.9%
data/restraints/parameters	824/4/33
goodness of fit on F^2	0.805
final R indices [$I > 2\sigma(I)$]	R_1 = 0.0235, wR_2 = 0.0342
R indices (all data)	R_1 = 0.0420, wR_2 = 0.0356
largest diff. peak and hole	0.851 and −1.575 e·Å^{-3}

$R_1 = \sum||F_o| - |F_c||/\sum|F_o|$
$wR_2 = [\sum(F_o^2 - F_c^2)^2/\sum(w \cdot F_o^2)^2]^{1/2}$
$w = (\sigma^2 \cdot F_o^2 + (aP)^2 + bP)^{-1}$, $P = [F_o^2 + 2F_c^2]/3$

The assignment of the occupancy of the metal sites deserves some attention. Each unit cell contains four M(1) sites, four M(2) sites, and two M(3) sites. Assigning the usual formal charges of −2 to the 18 Se atoms and +3 to the four P atoms gives a total charge of −24 to be compensated by the positive transition metal ions. The typical oxidation states of Ni^{2+} and Cr^{3+} then imply that there are four Cr atoms and six Ni atoms per unit cell. This gives the stoichiometry $Ni_3Cr_2P_2Se_9$.

The two metal sites M(1) and M(2) are in octahedral coordination, which is common for both Cr and Ni. The trigonal bipyramidal coordination of the third metal site M(3) is unusual for transition metals. Thus, on the basis of coordination environments alone, no conclusions can be drawn regarding the occupancy of these sites. Comparison of M−Se bond distances in Figure 2 shows that the two octahedral environments are essentially identical, which also

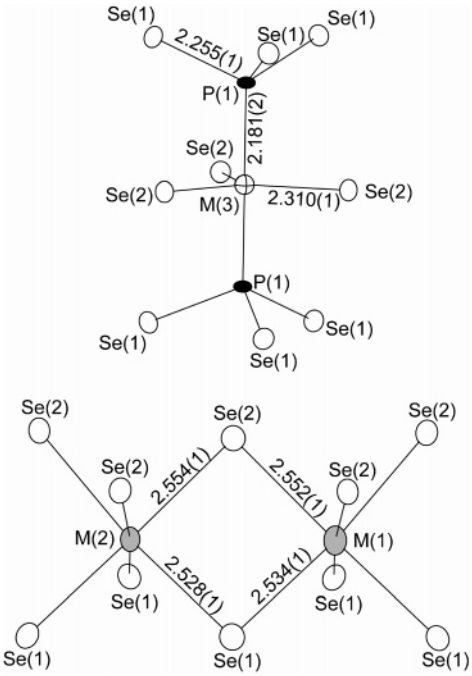

Figure 2. Coordination environments and displacement ellipsoids (95%) in $Ni_3Cr_2P_2Se_9$. Interatomic distances (Å) are labeled.

Table 2. Results from Refinement of Several Distributions of Ni and Cr Atoms on the Metal Sites M(1), M(2), and M(3) in $Ni_3Cr_2P_2Se_9$[a]

occupancy of M(1)	Cr	Ni	Ni/Cr 1:1	refined[b]
occupancy of M(2)	Ni	Cr	Ni/Cr 1:1	refined[b]
occupancy of M(3)	Ni	Ni	Ni	refined[b]
R1	0.0315	0.0316	0.0235	0.0232
wR2	0.0708	0.0857	0.0342	0.0329
M(1) *U*(eq)	0.001	0.013	0.006	0.006
M(2) *U*(eq)	0.011	0.000	0.005	0.006
M(3) *U*(eq)	0.005	0.005	0.005	0.004

[a] Each Column represents a different arrangement of Ni and Cr. [b] Mixture of Ni and Cr refined on all M sites, but with the total Ni:Cr ratio fixed at 3:2.

gives no insight into the correct occupancies, because Ni−Se and Cr−Se distances in sixfold coordination are very similar (2.50 in NiSe[7] and 2.51−2.54 in Cr_2Se_3[8]).

Comparisons of bond valence sums[9] can be helpful in determining site occupancies but in this case are inconclusive. Bond valence sums were calculated for both Ni and Cr at each of the three metal sites in the structure. The results showed that the bond valence sums for both are equally close to the expected values on all three metal sites (2 and 3 for Ni and Cr, respectively) and thus do not help in the assignment of occupancies.

We are therefore left with only the X-ray data to determine the atom assignments of the metal sites. However, because of the similar scattering power of the two types of atoms, refinement of the ratio of Ni:Cr on these sites is not straightforward. Various distributions of Ni and Cr atoms over the three metal sites which maintain charge balance were investigated, and the results are presented in Table 2. From this table it is clear that fully ordered arrangements of Ni and Cr are the least consistent with the X-ray data (higher *R* values, and displacement parameters which suggest the Ni site needs less scattering power and the Cr site needs more). This suggests that these two sites may be occupied by a mixture of Ni and Cr. It is common for Ni and Cr to share atomic sites because of their similar sizes (as in the sulfides $Ni_xCr_{3-x}S_4$[10] and the telluride $Ni_{0.3}Cr_{0.7}Te$[11]). Allowing mixtures of Ni and Cr on all three sites while maintaining charge balance (the rightmost column in Table 2) gives significantly lower *R* values and more reasonable displacement parameters than the ordered arrangements. The refined site occupancies (in the form Ni:Cr) were M(1) 50:50, M(2) 56:44, and M(3) 87:13. This is close to equal mixtures of Ni and Cr on the octahedral sites and pure Ni on the bipyramidal site. Table 2 shows that there is no significant difference in the quality of the refinement between this and the freely refined case. Therefore the model with M(1) and M(2) occupied by 50:50 mixtures of Ni and Cr and M(3) occupied by Ni is likely the best description of the structure that can be obtained from the present X-ray data.

The crystal used for the structure determination was merohedrally twinned; the twin law is a twofold rotation about the [110] direction and is common in hexagonal space groups which do not contain this operation as a symmetry element.[12] Refinement of the structure revealed a small amount of stacking fault type disorder in the crystal as well. See the Supporting Information for details regarding the twinning and disorder. The low level of the disorder in this particular crystal (~7%) allowed the structure to be solved and refined. Higher concentrations of such stacking faults can preclude structure determination. This is likely the source of the problems encountered with the sulfur analogue, $Ni_3Cr_2P_2S_9$, for which no good quality single-crystal diffraction data has been obtained. Indexing the single-crystal data for this compound proved difficult and did not consistently return the same cell parameters. The better data sets tended to give unit cell parameters close to $a = 5.9$ Å and $c = 18.0$ Å, but often the *c*-axis length was double or triple this value, likely a sign of stacking faults or possibly a supercell. Although the crystal structure of the sulfide could not be determined by single-crystal X-ray diffraction experiments, the powder X-ray diffraction (PXRD) results discussed below suggest that the sulfur and selenium analogues are isostructural.

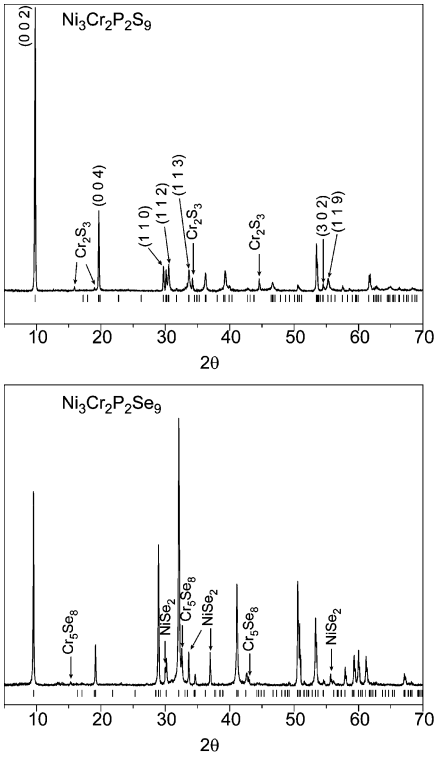

Figure 3. Measured PXRD patterns for $Ni_3Cr_2P_2S_9$ and $Ni_3Cr_2P_2Se_9$. Tick marks locate predicted peak positions based on refined lattice constants and using the space group $P6_3/m$ determined by single-crystal diffraction on $Ni_3Cr_2P_2Se_9$. Several single indexed lines in the $Ni_3Cr_2P_2S_9$ pattern are labeled with (*hkl*) values. Observed impurity peaks are also labeled.

Powder X-ray Diffraction: $Ni_3Cr_2P_2S_9$ and $Ni_3Cr_2P_2Se_9$. Measured PXRD patterns for $Ni_3Cr_2P_2S_9$ and $Ni_3Cr_2P_2Se_9$ are shown in Figure 3. Neither compound has been made as a single phase bulk sample. The data shown in Figure 3 represent two of the purest samples that have been synthesized (see Supporting Information for details). Binary transition metal chalcogenides (Cr_2S_3,[13] Cr_5Se_8,[14] and $NiSe_2$[15]) are present in these products as impurities.

(7) Rost, E.; Vestersjo, E. *Acta Chem. Scand.* **1968**, *22*, 2118.
(8) Adachi, Y.; Ohashi, M.; Kaneko, T.; Yuzuri, M.; Yamaguchi, Y.; Funahashi, S.; Morii, Y. *J. Phys. Soc. Jpn.* **1994**, *63*, 1548.
(9) O'Keeffe, M.; Brese, N. *J. Am. Chem. Soc.* **1991**, *113*, 3226.
(10) Colgan, D. C.; Powell, A. V. *J. Mater. Chem.* **1997**, *7*, 2433.
(11) Makovetskii, G. I.; Dymont, V. P. *Physica Status Solidi A* **1985**, *85*, 69.
(12) Parsons, S. *Acta Crystallgr., Sect. D* **2003**, *59*, 1995.
(13) Jellinek, F. *Acta Crystallogr.* **1957**, *10*, 620.

Measured peak positions in these patterns were used to refine the lattice constants of each phase at room temperature. The results for $Ni_3Cr_2P_2Se_9$ were $a = 6.253(1)$ Å and $c = 18.494(4)$ Å, in good agreement those determined by single-crystal diffraction shown in Table 1. The results for $Ni_3Cr_2P_2S_9$ were $a = 5.934(1)$ Å and $c = 18.053(4)$ Å. These are smaller than the lattice constants of the Se compound, as expected when Se is replaced by the smaller S, and are in good agreement with the unit cell suggested for $Ni_3Cr_2P_2S_9$ by single-crystal diffraction experiments noted above. Peak positions calculated using the refined unit cell constants and the space group $P6_3/m$ are shown in Figure 3 and are seen to account for all observed reflections other than those from the impurity Cr_2S_3. These observations strongly suggest that the sulfide and selenide are isostructural. PXRD from samples with nominal compositions $Ni_3Cr_2P_2S_{9-x}Se_x$ showed systematic shifts of the peak positions with x, suggesting that a full solid solution exists.

Several of the single indexed reflections from $Ni_3Cr_2P_2S_9$ are labeled by their *hkl* values in Figure 3. Reflections of the form (00*l*) and (*hk*0) are sharp, while reflections of the form (*hkl*) are significantly broadened. This is typical of layered materials which contain stacking faults, displacements of the layers perpendicular to the stacking direction.[16] It is likely that stacking faults are responsible for the difficulty in obtaining good single-crystal X-ray diffraction data from crystals of $Ni_3Cr_2P_2S_9$.

Thermoelectric Properties of $Ni_3Cr_2P_2S_{9-x}Se_x$. Transport property measurements were performed using a home-built apparatus[17] on platelet single crystals from the reaction of stoichiometric mixtures of the elements which targeted the compositions $Ni_3Cr_2P_2S_{9-x}Se_x$ for $x = 0$, 3, 6 (see Supporting Information for further details). The results of the resistivity and Seebeck coefficient measurements are shown in Figure 4. The small size of the crystals precluded thermal conductivity measurements using our apparatus. In Figure 4 the samples are labeled by these nominal compositions. Energy dispersive electron microprobe analysis of the crystals used for the measurements confirmed their composition to be $Ni_3Cr_2P_2S_{9-x}Se_x$. The approximate values of x determined from the microprobe measurements were 4 and 7 for the crystals with nominal $x = 3$ and 6, respectively.

The dependence of the thermoelectric properties on x is not systematic. The $x = 3$ sample has higher value of S and ρ than both the $x = 0$ and $x = 6$ samples. The resistivity of all three materials decreases with increasing temperature, with room-temperature values on the order of 100 mΩ·cm. This is 2 orders of magnitude higher than typical good thermoelectric materials. The Seebeck coefficients are positive, indicating p-type behavior. At 300 K the $x = 3$ sample has moderately high thermopower, close to that of optimized Bi_2Te_3-based alloys, which have $S \approx 220$ μV/K and $\rho \approx 1$ mΩ·cm near room temperature.[18] However, the high values of ρ for $Ni_3Cr_2P_2S_{9-x}Se_x$ make all of these compounds unsuitable for thermoelectric applications as prepared. Suitable doping could significantly decrease the electrical resistivity; however, increasing the carrier concentration typically decreases the Seebeck coefficient, and so it is unlikely that doping these materials will produce a good p-type thermoelectric material. It is possible that n-type doping would result in better thermoelectric properties.

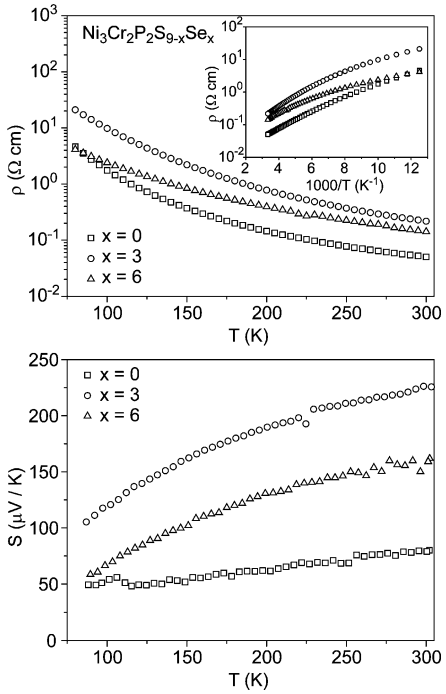

Figure 4. Measured resistivity ρ and Seebeck coefficient S of three members of the solid solution series $Ni_3Cr_2P_2S_{9-x}Se_x$ labeled by their nominal compositions. The estimated uncertainty on these measurements is ±10%.

The nonlinear behavior of log(ρ) versus $1/T$ seen in the inset of Figure 4 shows that the resistivity is not well described by a simple activation law over the entire temperature range. However, between 200 and 300 K the resistivity data from all three samples can be fit to activated models giving activation energies of 0.02−0.03 eV. Temperature-dependent mobilities or multiple sources of activated carriers may be responsible for the deviation from linearity in log(ρ) versus $1/T$ below 200 K. The behavior at the lowest temperatures investigated is likely also influenced by the onset of magnetic ordering which is observed near 105 K in $Ni_3Cr_2P_2S_9$ (vida infra).

Magnetic Properties of $Ni_3Cr_2P_2S_9$. A Quantum Design Magnetic Properties Measurement System (SQUID magnetometer) was used for magnetic characterization of oriented single crystals of $Ni_3Cr_2P_2S_9$. It is expected that the complex crystal structure of this compound may lead to complicated magnetic behavior. Although no single-crystal structure has been obtained for $Ni_3Cr_2P_2S_9$, it is expected to be isostructural with the selenide analogue (vida supra), which contains double layers of transition metal ions arranged in honeycomb nets perpendicular to the *c*-direction (Figure 1). The structure

(14) Wehmeier, F. H.; Keve, E. T.; Abrahams, S. C. *Inorg. Chem.* **1970**, *9*, 2125. Huppertz, H.; Luehmann, H.; Bensch, W. *Z. Naturforsch. B* **2003**, *58*, 934.
(15) Groenvold, F.; Jacobsen, E. *Acta Chem. Scand.* **1956**, *10*, 1440.
(16) Guinier, A. *X-ray Diffraction in Crystals, Imperfect Crystals, and Amorphous Bodies*; W. H. Freeman and Company: New York, 1963.
(17) Reynolds, T. K.; McGuire, M. A.; DiSalvo, F. J. *J. Solid State Chem.* **2004**, *177*, 3038.
(18) Yim, W. M.; Rosi, F. D. *Solid-State Electron.* **1972**, *15*, 1121.

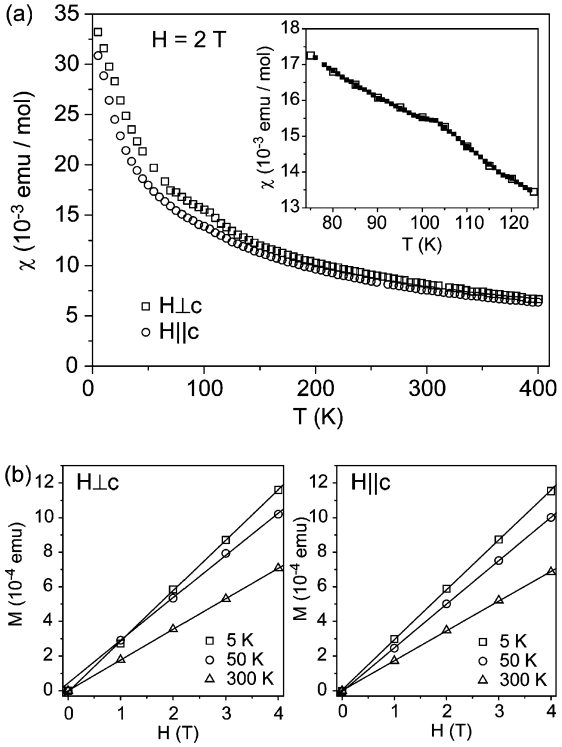

Figure 5. (a) Magnetic susceptibility per mole of formula units of $Ni_3Cr_2P_2S_9$ crystals (corrected for sample holder and core diamagnetic contributions) between 5 and 400 K with the applied field of 2 T parallel and perpendicular to the *c*-axis. The inset shows the cusp near 105 K in $\chi_\perp$ measured on two separate runs. (b) The field dependence of the measured magnetic moment (not corrected for the sample holder contribution). The linear fits to all curves show paramagnetic behavior with the exception of that measured with *H* in the *ab*-plane at 50 K, for which the linear fit to the data between 1 and 4 T is shown.

Ni^{2+} ions in trigonal bipyramidal coordination on the M(3) site are not considered in the analysis of the magnetic data because they are not expected to have a local moment ($S = 0$). In the selenide, the shortest M−M distance is 3.2 Å and is along the *c*-direction, between M sites in neighboring honeycomb nets within a double layer. The next shortest is in the *ab*-plane, between M sites within a single honeycomb net, and is 3.6 Å. The shortest distance along c between M atoms in neighboring double layers is 6.0 Å. Magnetic interactions are further complicated by the mixed occupancy of two of the three M sites by Cr and Ni, resulting in varying local magnetic environments for a single crystallographic site in the average structure.

Figure 5a shows the temperature dependence of the magnetic susceptibility ($\chi = M/H$) per formula unit determined from magnetization measurements in an applied field of $H = 2$ T aligned parallel and perpendicular to the *c*-axis. Little anisotropy is observed in the susceptibility data shown in Figure 5a, and a subtle but reproducible cusp is observed near 105 K. The field dependence of the magnetic moment of the $Ni_3Cr_2P_2S_9$ crystals is shown in Figure 5b. The lines are linear fits to the *M* versus *H* data. The linear behavior is observed up to 5 T in all cases except at 50 K with $H \perp c$. In this case the line shown on the plot is a fit to the data only for $H \geq 1$ T. This behavior may be related to the cusp near 105 K in the χ vs *T* data, which is more pronounced in the $H \perp c$ data than that collected with $H \parallel c$ (Figure 5a).

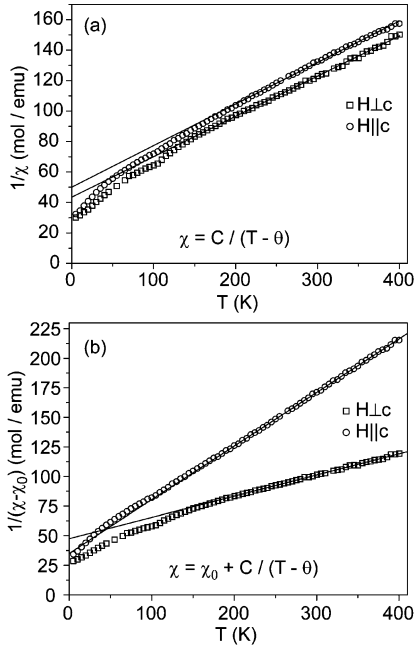

Figure 6. Fits to the susceptibility data shown in Figure 5 between 200 and 400 K using (a) the Curie−Weiss law and (b) a modified Curie−Weiss law which includes a temperature-independent term.

Figure 6a shows $1/\chi$ as a function of *T*, along with linear fits to the data between 200 and 400 K. Significant deviation from Curie−Weiss behavior [$\chi = C/(T - \theta)$] is observed at lower temperatures, in part due to the cusp observed at 105 K. The fits give Curie constants (*C*) of 4.0 emu·K/mol and 3.9 emu·K/mol and Weiss temperatures (θ) of −180 K and −200 K for data collected with $H \perp c$ and $H \parallel c$, respectively. The large negative values of θ suggest strong antiferromagnetic interactions. Each formula unit contains two $S = 3/2$ Cr^{3+} ions, two $S = 1$ Ni^{2+} ions, and one $S = 0$ Ni^{2+} ion (in trigonal bipyramidal coordination). From this an expected Curie constant of 5.75 emu·K/mol is calculated. This is significantly higher than the values of *C* determined from the fits in Figure 6a.

Inspection of the fits to the $1/\chi$ data shown in Figure 6a reveals systematic deviations from the simple Curie−Weiss law, most noticeable for $H \parallel c$. Because of this, fitting was also performed with the addition of a temperature-independent term to the Curie−Weiss model, using the equation $\chi = \chi_0 + C/(T - \theta)$. The results are shown in Figure 6b and the fitted parameter values are $\chi_{0\perp} = -1.7 \times 10^{-3}$ emu/mol, $C_\perp = 5.6$ emu·K/mol, $\theta_\perp = -260$ K; $\chi_{0\parallel} = 1.7 \times 10^{-3}$ emu/mol, $C_\parallel = 2.2$ emu·K/mol, $\theta_\parallel = -80$ K. In contrast to the fit using simple Curie−Weiss model described above and shown in Figure 6a, this analysis, with the inclusion of a temperature-independent term, suggests strong anisotropy in both the magnetic interactions (θ) and the moments (*C*). The origin of the relatively large values χ_0 and the reason for its difference in sign for the two crystal orientations are unclear. The need for such large temperature-independent terms to describe the data using a Curie−Weiss model may suggest that significant magnetic correlations persist up to 400 K or simply that this model is incapable of describing the complex magnetic interactions in $Ni_3Cr_2P_2S_9$.

We propose three possible explanations for the observed deviation from Curie−Weiss behavior (Figures 5a and 6) at

temperatures below about 150 K. First, possible contamination by magnetic impurities must be always be considered. Although the magnetic measurements were performed on single crystals, the crystals were selected from a multiphase reaction product. Electron microprobe analysis confirmed that the selected crystals were $Ni_3Cr_2P_2S_9$, and careful inspection under an optical microscope showed no observable contamination. However, it is interesting to note that Cr_2S_3 has magnetic properties in some ways similar to those observed in the present study. Cr_2S_3 undergoes a ferrimagnetic transition at $T_N = 118$ K.[19,20] As expected for a ferrimagnet, $M(H)$ curves for Cr_2S_3 show linear behavior for $T > T_N$ and rapid saturation followed by a linear increase for $T < T_N$.[20] Similar behavior in $M(H)$ was noted at 50 K (but not 5 K) in $Ni_3Cr_2P_2S_9$ in Figure 5b. The magnetization of Cr_2S_3 increases abruptly as T is lowered below T_N.[19,21,22] A larger increase is seen when H is perpendicular to the hexagonal c-axis than when H is aligned with c, and the magnitude of the anisotropy depends on the stoichiometry of the compound.[22] We estimate that contamination by as little as 5% of Cr_2S_3 by weight could produce an increase in magnetization similar in magnitude to that associated with the cusp shown in Figure 5a.

Second, if the observed cusp in the $\chi(T)$ data near 105 K is an intrinsic property of $Ni_3Cr_2P_2S_9$, it is likely a signature of an antiferromagnetic ordering transition. The continued increase in χ upon further cooling may indicate canting of the moments in the ordered state. A cusp in $\chi(T)$ similar to that observed for $Ni_3Cr_2P_2S_9$ has been observed in the binary compound CrSe,[23,24] which has been shown to adopt a noncolinear antiferromagnetic spin arrangement below about 300 K.[25]

Finally, the cusp near 105 K and paramagnetic behavior at lower temperatures may indicate that an antiferromagnetic ordering takes place near 105 K, but not all of the magnetic moments participate. This may suggest that only one of the several types of magnetic interaction in this compound order at this temperature or that ordering occurs only for certain local arrangements of Ni and Cr on the mixed transition metal sites.

The layered crystal structure of this material may inhibit long-range magnetic ordering and be in part responsible for the persistence of paramagnetic behavior in $Ni_3Cr_2P_2S_9$ at low temperatures. It has been shown that no ordered antiferromagnetic (or ferromagnetic) ground states exist for isotropic one- and two-dimensional Heisenberg models.[26] However, most layered materials do undergo ordering transitions. These are usually attributed to interlayer coupling which makes the magnetic system three-dimensional or to anisotropic intralayer couplings which have been shown to lead to ordered states through the so-called Kosterlitz and Thouless (KT) transition.[27] For example, $BaNi_2V_2O_8$ has honeycomb nets of magnetic Ni atoms in edge sharing NiO_6 octahedra which are separated from neighboring nets by Ba atoms and VO_4 tetrahedra. This compound orders antiferromagnetically at 50 K[28] in what is believed to be a KT transition.[29] Another, perhaps more closely related, example is $NiPS_3$, which is made up of layers or edge sharing NiS_6 octahedra which form a honeycomb net with P−P dimers in the holes forming ethane-like P_2S_6 units.[6] $NiPS_3$ orders antiferromagnetically at 155 K, and its magnetic susceptibility exhibits a broad maximum above this transition, centered near 270 K.[30] Further study, perhaps through neutron diffraction experiments, is needed to gain a deeper insight into the magnetic behavior of $Ni_3Cr_2P_2S_9$ and $Ni_3Cr_2P_2Se_9$.

Conclusions

The new quaternary compounds $Ni_3Cr_2P_2S_9$ and $Ni_3Cr_2P_2Se_9$ have been synthesized and characterized. Investigation of mixed sulfide−selenide compositions suggest that a complete solid solution exists. Transport properties measurements show the materials to be p-type semiconductors with small band gaps or activation energies. In addition, interesting structural and magnetic properties were observed. The structures of these compounds contain unusual five-coordinate Ni atoms and a new type of layer never before observed in transition metal chalcogenides. These layers can be derived by fusing two layers of the $NiPS_3$ structure through face sharing of the NiS_6 octahedra, replacing the P−P dimers with linear P−Ni−P units, and distributing Ni and Cr evenly over the octahedral sites. The initial study of the magnetic properties of the sulfide revealed interesting behavior indicating complex magnetic interactions and suggest that an antiferromagnetic ordering transition, possibly into a canted state, occurs near 105 K. These observations suggest further studies of the magnetic properties of $Ni_3Cr_2P_2S_9$ and $Ni_3Cr_2P_2Se_9$ are warranted.

Acknowledgment. This work was funded Cornell University and by NSF Grant DMR-0011572. We gratefully acknowledge helpful discussions with Dr. Thomas K. Reynolds and Dr. Craig M. Downie. We thank Jonathon Petrie and Dr. Hideki Abe for help with the magnetization measurements, Dr. Emil B. Lobkovsky for assistance in collecting single-crystal X-ray diffraction data, and John Hunt for guidance in using the electron microprobe facility in the Cornell Center for Materials Research which is supported through a MRSEC Grant (DMR-520404).

Supporting Information Available: Experimental details (PDF) regarding synthesis, characterization, and crystal structure refinement (including a CIF file for $Ni_3Cr_2P_2Se_9$). This material is available free of charge via the Internet at http://pubs.acs.org.

CM070849F

(19) Sugiura, T.; Iwahashi, K.; Masuda, Y. J. *Phys. Soc. Japan.* **1972**, *33*, 1172.
(20) Vaqueiro, P.; Powell, A. V.; Coldea, A. I.; Steer, C. A.; Marshall, I. M.; Blundell, S. J.; Singleton, J.; Ohtani, T. *Phys. Rev. B* **2001**, *64*, 132402.
(21) Vaqueiro, P.; Powell, A. V.; Coldea, A. I.; Steer, C. A.; Marshall, I. M.; Blundell, S. J.; Singleton, J.; Ohtani, T. *Phys. Rev. B* **2001**, *64*, 132402.
(22) Mikiami, M.; Igaki, K.; Ohashi, N. *J. Phys. Soc. Jpn.* **1972**, *32*, 1217.
(23) Tsubokawa, I. *J. Phys. Soc. Jpn.* **1956**, *11*, 662.
(24) Tsubokawa, I. *J. Phys. Soc. Jpn.* **1960**, *15*, 2243.
(25) Corliss, L. M.; Elliott, N.; Hastings, J. M.; Sass, R. L. *Phys. Rev.* **1961**, *122*, 1402.
(26) Mermin, N. D; Wagner, H. *Phys. Rev. Lett.* **1966**, *17*, 1133.
(27) Kosterlitz, J. M.; Thouless, D. J. *J. Phys. C* **1973**, *6*, 1181.
(28) Rogado, N.; Huang, Q.; Lynn, J. W.; Ramirez, A. P.; Huse, D.; Cava, R. J. *Phys. Rev. B* **2002**, *65*, 144443.
(29) Heinrich, M.; von Nidda, H. A.; Loidl, A.; Rogado, N.; Cava, R. J. *Phys. Rev. Lett.* **2003**, *91*, 137601.
(30) Joy, P. A.; Vasudevan, S. *Phys. Rev. B* **1992**, *46*, 5425.